ARTICLE

Effect of Orientation on Plasmonic Coupling between Gold Nanorods

Christopher Tabor, Desiree Van Haute, and Mostafa A. El-Sayed*

School of Chemistry and Biochemistry, Georgia Institute of Technology, 770 State Street, Atlanta, Georgia 30332

ABSTRACT Radiative coupling of induced plasmonic fields in metal nanoparticles has drawn increasing attention in the recent literature due to a combination of improved experimental methods to study such phenomena and numerous potential applications, such as plasmonic nanoparticle rulers and plasmonic circuitry. Many groups, including ours, have used a near-exponential fit to express the size scaling of plasmonic coupling. First, we show experimental agreement between previously simulated nanorod coupling and plasmonic coupling in electron beam lithography (EBL) fabricated nanorods using the near-exponential expression. Next, we study the effect of nanoparticle orientation on plasmonic coupling using EBL and DDA simulations. We develop a mathematical relationship that is consistent with our findings and quantitatively describes plasmonic coupling between nanorods as a function of orientation, separation, induced dipole strength, and the dielectric constant of the medium. For applications utilizing plasmonic coupling to become viable with particle shapes that do not have spherical symmetry, such as nanoprisms and nanorods, comparison of the experimental and theoretical results of how particle orientation affects plasmonic coupling is essential.

KEYWORDS: plasmon · nanorod · orientation · nanoparticle · EBL · hybridization · DDA

Noble metal nanoparticles are exciting materials because their conduction band electrons couple with light in the visible to near-IR region of the electromagnetic spectrum. The electric field of the light induces a coherent oscillation of electrons on the surface of the particle that is resonant with the excitation frequency. The resonance reaches a maximum value at specific frequencies, identified as dipole, quadrupole, *etc.* For particles that are small with respect to the wavelength of light ($r < 1/4*\lambda$), the dipole resonance dominates the spectral signature of the particle. The resonant energy of this dipole transition in a single nanoparticle is a function of the dielectric medium in which the nanoparticle is embedded, the shape and size of the nanoparticle, and the specific plasmonic metal. By changing these variables, one can tune the optical properties of a single noble metal nanoparticle. This tunability of the localized surface plasmonic resonance (LSPR) frequency and the intense localized field induced at the nanoparticle surface in noble metal nanoparticles gives them enormous potential in medical,[1−3] optical,[4−7] and sensor[8−12] applications.

As two particles approach one another, the intense near-fields at the surface of the particles overlap and couple with one another, strongly affecting the plasmonic resonance energies. The coupling between two degenerate plasmonic modes has been discussed as an analogy to molecular exciton coupling theory (MECT),[13−16] which describes the splitting of an excited state energy level into two eigenmodes, one at higher energy and one at lower energy, whose separation is approximated by the Simpson−Peterson equation. Similarly, when two nanoparticles come into contact with one another, the individual dipole modes couple to produce two new dipole resonances, one at a higher energy and one at a lower energy, associated with the dimer system. For tip-to-tip oriented rods, the higher energy hybrid dipole is forbidden, due to the net dipole being equal to zero. The lower energy hybrid dipole is stronger in intensity, and the fractional shift in the resonance wavelength is a measure of the degree of coupling between the two particles.

While there are commonalities between the Simpson−Peterson approximation with near-field coupling of plasmonic nanoparticles, this model assumes that the excitation is a single dipole state, and the coupling occurs only between these two dipoles. Plasmonic excitations, while predominantly dipolar at large separations, have contributions from higher order multipoles, as well, especially at decreasing separations. These higher order resonances can be seen clearly in anisotropic particles

*Address correspondence to melsayed@gatech.edu.

Received for review July 10, 2009 and accepted October 26, 2009.

Published online November 5, 2009. 10.1021/nn900779f CCC: $40.75

such as nanoprisms.[17,18] This point has been evidenced in the literature by numerous researchers that fit the decay of the plasmonic field coupling with separation to an exponential function instead of the R^{-3} functional dependence predicted by the dipole−dipole model.[15,19,20] In these papers, the exponential fit is only used to approximate the functional dependence of the dipole coupling on separation and should be used prudently because the exponential fit to the data in the range of $1.5 \times S \leq R \leq 2.5 \times S$ and $R \leq 1.1 \times S$ is poor. However, the near-exponential description of the plasmonic coupling does facilitate its application by providing a straightforward model that expresses the relationship, and this model has been used to predict the separation of plasmonic nanoparticles using their optical signal.[21]

The shift in the resonance energy with decreasing interparticle separation was first studied by Su *et al.*[20] and Rechberger *et al.*,[22] who independently demonstrated that near-field coupling red shifts the dipole resonance frequency. The near-field coupling was quantitatively measured by the fractional shift in the dipole resonance wavelength ($\Delta\lambda/\lambda$), which decayed near-exponentially with separation. Later, the exponential decay length (τ) in units of the particle size was found to be consistent among several nanoparticle shapes[21,23,24] (eq 1), such as nanospheres, nanodiscs, and nanoshells.

$$\left(\frac{\Delta\lambda}{\lambda}\right) = A \times e^{\left(\frac{-s/D}{\tau}\right)} \quad (1)$$

Here, λ is the wavelength plasmonic resonance wavelength of the single nanoparticle, $\Delta\lambda$ is the shift in the plasmonic resonance wavelength of the nanoparticle dimer with respect to the single nanoparticle, τ is the exponential coupling decay length of the dimer, A is a pre-exponential fitting factor, s is the separation between nanoparticles, and D is the physical size of the nanoparticle.

This method of describing the plasmonic coupling as a near-exponential function of separation was an attempt to simplify the convoluted coupling that occurs between not only plasmonic dipoles (which theoretically couple as a function of separation such as R^{-3}) but also higher order multipoles as the separation decreases. This near-exponential trend also highlighted the common size scaling of many symmetric nanoparticle shapes by reporting the exponential decay length of the coupling (τ) in units of the particle size and the commonality of this value for various nanoparticle sizes. It was first postulated that this exponential decay length was universal for all shapes of nanoparticles; however, it has since been shown in the literature that this value can vary with particle shape and is larger for some shapes, such as the nanoprisms.[17]

While these studies have investigated the coupling between two plasmonic nanoparticle dimers, they have all been limited in scope to ideally oriented particles, save for two recent publications.[19,25] In the first work, Funston *et al.*[19] found a nice correlation between the single particle/dimer optical signal of distributed colloidal nanorod dimers and DDA simulations of various orientations. They found that for very small separations ($R/S < 0.09$) the exponential fit is not accurate. In addition, some very nice hybridization schemes were presented for particular orientations of nanorods with respect to one another. In the second article, Willingham *et al.*[25] theoretically compared a plasmonic hybridization calculation to FDTD calculations in order to investigate plasmonic coupling in two nanorods. For applications such as the plasmonic ruler[26] and subwavelength optics,[27−29] it is helpful to investigate the plasmonic near-field coupling of nanoparticles with anisotropic shapes when the orientation is systematically varied and at larger separations.

In this paper, we use electron beam lithography to form two-dimensional arrays of pairs of nanorods with different distances and orientation and measure the positions of their surface plasmon extinction. We discuss the observed plasmonic coupling in nanorod dimers, with systematically varied separations and rotational geometries, in order to understand and model the coupling between less than ideally oriented anisotropic nanorods, specifically when one rod is rotated around its center of mass. We discuss the advantages of modeling plasmonic coupling with the plasmonic hybridization model (the analogue to MECT) and modify the Simpson−Peterson approximation to incorporate the plasmonic near-field coupling dependence on four variables; separation, orientation, induced dipole size, and medium dielectric. We also discuss previous observations of nanoprisms that possess a stronger coupling at larger distances compared with discs and spheres of the same size as additional support for the model.

RESULTS AND DISCUSSION

Tip-to-Tip Coupling between Nanorods. We first investigated nanorods oriented tip-to-tip and the relationship between interparticle separation and the degree of coupling between the longitudinal plasmon resonances. This has previously been studied qualitatively in colloidal solutions[13,30,31] and quantitatively through DDA simulations[19,24] but has not yet been systematically reported experimentally. A few representative SEM images of the nanorod dimers oriented tip-to-tip are shown in Figure 1A−C. Statistical measurements were performed on all of the nanorod arrays to ensure that the size distribution was homogeneous. The average magnitude for the length and width of the nanorods was 66.4 ± 1.7 and 37.6 ± 1.8 nm, respectively, and the thickness was 18 nm. By measuring the extinction spectra of the nanorod dimers, we verified that the plasmonic coupling obeys the predicted red shift in a near-exponential fashion. The experimental data points are

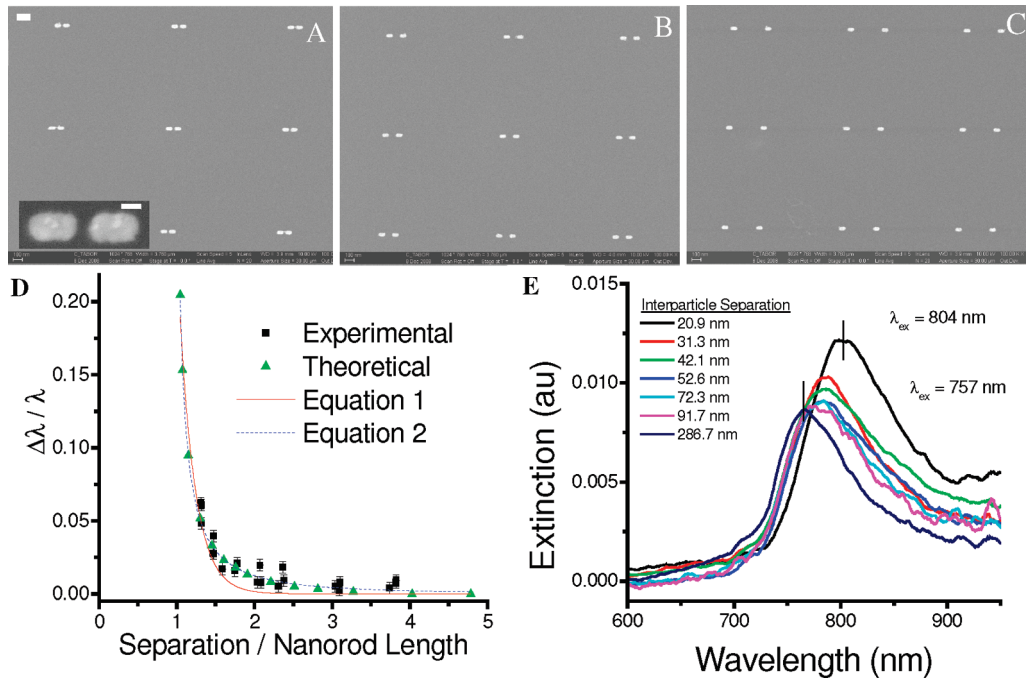

Figure 1. (A−C) SEM images of gold nanorod dimer arrays fabricated by EBL with various interparticle separations: 20.9, 72.3, and 286.7 nm. The scale bar in the top left corner of A is 100 nm. The inset in A is a 400k× magnification of a nanorod dimer. The scale bar in the inset is 30 nm. (D) Plasmonic coupling (Δλ/λ) shown as a function of interparticle separation in units of the nanorod length for experimental EBL fabricated (black squares) and DDA simulated particles (green prisms). Two fits are presented, the exponential model with a decay length of $\tau = 0.20$ (red solid line) and a derived fit shown in eq 2 of the paper (blue dashed line). (E) Experimental extinction spectra of seven different nanorod dimers showing the spectral plasmonic shift from 757 to 804 nm.

shown in Figure 1D (black squares), and a DDA simulation of the exact particle size and shape is shown for completion (green triangles). Using the best-fit exponential function shown in eq 1, the decay length was confirmed to be $\tau = 0.20 \pm 0.03$, in agreement with previous simulations[24] (dashed blue line). Figure 1E shows the experimental extinction spectra of seven nanorod samples with varying interparticle separation.

While the exponential fit has been used to nearly approximate the decay of plasmonic coupling with separation, it has consistent deviations from the data, which have been discussed previously. A more accurate relationship has been derived in the Supporting Information of ref 21. This functional relationship between the fractional shift in the resonance wavelength and the separation between particles is presented in eq 2:

$$\left(\frac{\Delta\lambda}{\lambda}\right) = \frac{1}{\left(12\Lambda\left(1 + {}^{R}/_{S}\right)^{3} - (1 + \gamma)\right)} \qquad (2)$$

where Λ and γ are shape factors that are determined by the shape and size of the plasmonic nanoparticle, R is the separation between the centers of the plasmonic fields (typically approximated as the centers of the nanoparticles), and S is the size of the nanoparticle. Figure 1D shows a second best-fit line using eq 2 (blue dashed line), which has a much better fit to the data, both experimental and theoretical, compared with the exponential fit. The comparison between these two fits demonstrates two points: (1) the approximation of the exponential model in predicting separations between nanoparticles and (2) the necessity for a better mathematical description of the plasmonic field coupling as a function of particle separation. While the exponential

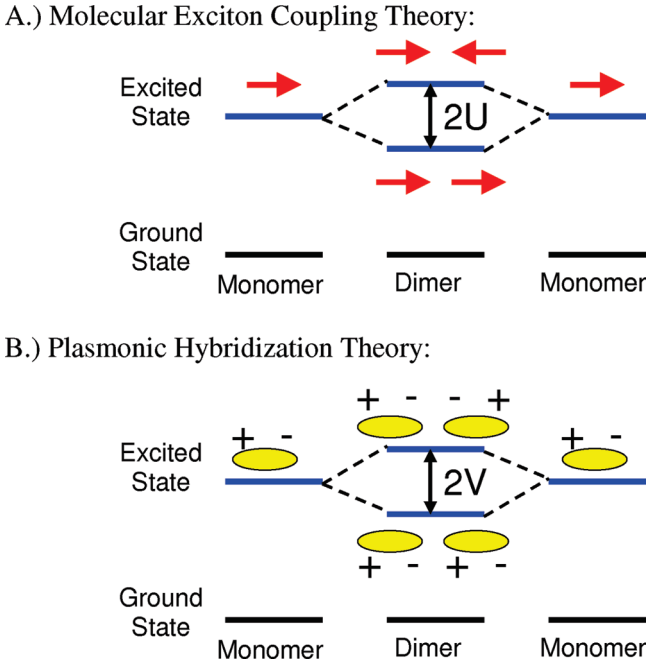

Figure 2. (A) Molecular exciton coupling theory (MECT) scheme depicting hybridized excited energy levels separated by 2U, where U is given in eq 3. (B) Plasmonic hybridization theory (PHT) scheme depicting the analogous hybridized excited energy levels separated by 2 V, where V is given below in eq 10.

decay model has been used to successfully approximate plasmonic coupling,[21] we point out here that a more accurate mathematical relationship, such as eq 2, would provide a better fit and be an improvement in the critical regions such as center-to-center separations of 1.5−2.5 in units of the particle size. An interesting note is that the parameter Λ is equal to 1/3 in the fit using eq 2, which is nearly the value predicted for a nanorod of this size (Λ = 1/aspect ratio). The small divergence probably exists due to the shape not being an ideal oblate spheroid, but a flattened rod.

According to MECT, the energy splitting (2U) between two hybridized modes was originally discussed for molecular dipole excitations by Kasha *et al.*[16] and is given by the Simpson−Peterson approximation[15] (eq 3)

$$U = \frac{|\mu^2|}{\eta^2 \times R^3} \times |\kappa| \qquad (3)$$

where μ is the transition dipole moment of the system, η is the refractive index of the medium, R is the center-to-center separation between dipoles, and κ is an orientation factor. Previously, plasmonic coupling has been qualitatively described using a hybridization model analogous to MECT,[14,19] shown in Figure 2. An analogous equation to the Simpson−Peterson approximation is developed here that quantitatively describes the hybridized energy levels using independent variables, separation (R), dipole module (μ), medium refractive index (η), orientation (κ). The Simpson−Peterson approximation will be used as a starting point for the development of such an equation.

On the Role of Nanoparticle Orientation on Plasmonic Field Coupling. Next, we report on the plasmonic coupling between nonideally oriented nanorods. The anisotropic nature of the nanorod and other anisotropic nanoparticle shapes could lead to superior plasmonic applications,[19] like the plasmon ruler and plasmonic waveguides. However, for anisotropic nanoparticles to be useful in plasmonic applications, the coupling must be understood as a function of particle orientation. We systematically studied the normalized optical extinction of the nanorod dimer pairs with polarized light along the interparticle axis with one nanorod positioned at varying angular orientations with respect to the interparticle axis. Representative SEM images of the nanorod dimers at different orientations are presented in Figure 3. The extinction wavelength for each rotation in Figure 3 was measured using a microspectrometer, and the spectra are shown in Figure 4A. As one of the nanorods is rotated around its center of mass and the incident polarization is held constant along the interparticle axis, the hybridized plasmonic dipole along the interparticle axis blue shifts as the coupling between the nanorods is reduced.

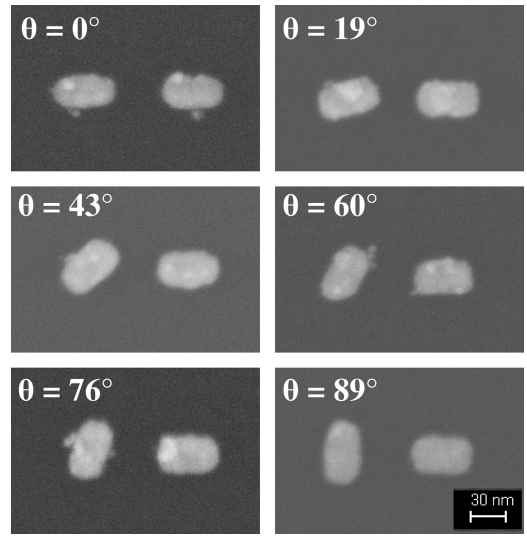

Figure 3. SEM images of nanorod samples fabricated by EBL with one rod rotated with respect to the interparticle axis by various angles (θ) indicated in the top left corner of each image.

The localized surface plasmon resonance is strictly a surface event, whereby the conduction band electrons oscillate in resonance on the surface of the nanoparticle. Therefore, we investigate the possibility that the decoupling of the plasmonic modes as one rod is rotated is due to a resulting increase in separation between the nanorod surfaces. The experimental data depicting the relationship between plasmonic coupling and the minimum surface-to-surface separation are plotted in Figure 4B. The data for the unrotated nanorod dimers with increasing separation are plotted with black squares. The red line is the best-fit curve in this region. The blue diamonds are the smallest surface-to-surface separation in the nanorod dimers where one rod is rotated. A linear best-fit line is shown in blue for the eye to follow. It is clear from these data that the plasmonic coupling dependence on orientation is distinct from the dependence on strict surface-to-surface separation.

The relationship between the angle of rotation and the fractional shift in the wavelength is shown in Figure 4C. The experimental data points are shown as black squares, and the DDA simulations are shown in green triangles. The fractional wavelength shift is normalized to the maximum shift (0, 180, and 360°), and the red line is the best-fit $\cos^2\theta$ function, with an R^2 fitting value of 1.00 and 0.96 for the simulated and experimental data, respectively. We note here that the data was also fit to a $\cos\theta$ function, but the agreement with the data was much poorer.

This relationship can be explained using the orientation factor (κ) presented in the Simpson−Peterson approximation in MECT

$$\kappa = \cos\theta_{12} - 3\cos\theta_{1R}\cos\theta_{2R} \qquad (4)$$

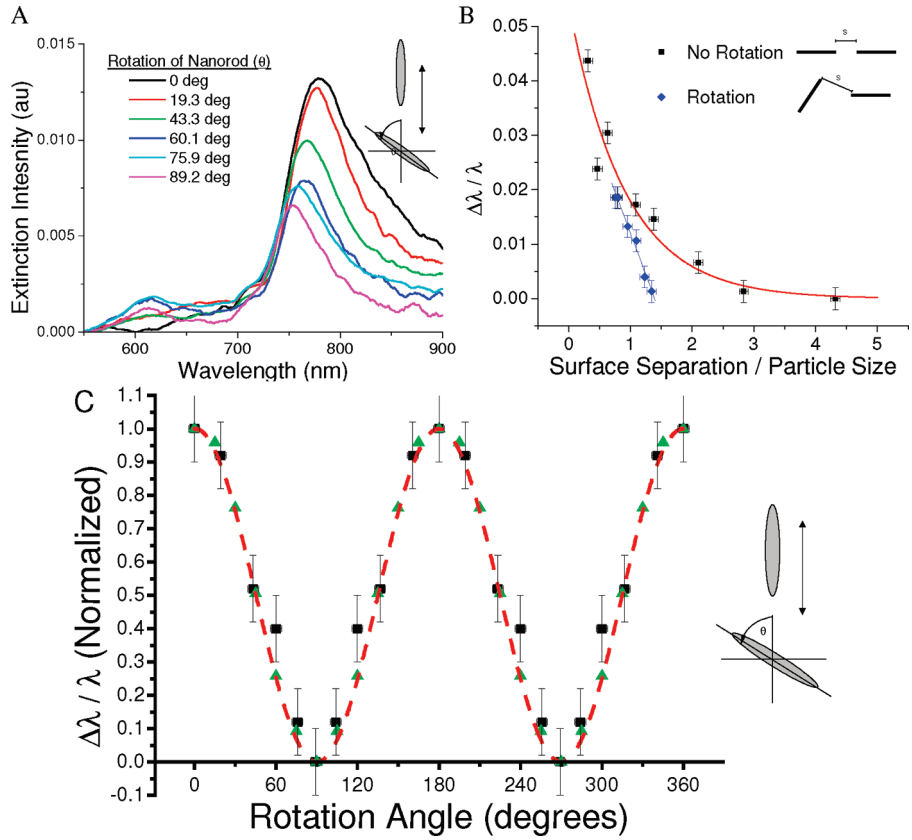

Figure 4. (A) Optical extinction of two gold nanorods separated by a center-to-center distance of 110 nm with various relative orientations. The light is polarized parallel to the interparticle axis, as is depicted in the inset, while one nanorod is rotated by some angle (θ) from the interparticle axis. When θ = 0°, the long axes of the nanorods are parallel, and when θ = 90°, the long axes of the nanorods are perpendicular. (B) Fractional wavelength shift of the coupled nanorods as a function of surface-to-surface separation. The blue data points are the nearest separation between the nanoparticle surfaces as one nanoparticle is rotated, indicating that the coupling is not functionally dependent on the surface-to-surface separation. (C) Experimental (black squares) and simulated (green triangles) plasmon coupling between two nanorods as a function of relative rotation of one nanorod around its center of mass. The plasmon coupling dependence follows a $\cos^2\theta$ dependence due to the coupling of the vector components of the dipole plasmons along the interparticle axis. The best-fit functional dependence is $(\Delta\lambda/\lambda) \propto \cos^2(\pi^*\theta/w)$, with an R^2 = 0.96 and 0.99 for the experimental and simulated data, respectively.

The value θ_{12} is the angle between the two dipole vectors, and the values θ_{1R} and θ_{2R} are the angles between respective dipole vectors 1 and 2 and the interparticle axis that connects the dipole centers. In the case presented here, κ is simplified to $\kappa = -2\cos\theta$, where θ is the rotation of one nanorod around a fixed point with respect to the interparticle axis.

Additionally, when the light is polarized along a fixed direction, as is the case in both the DDA simulation and the experimental work presented here, the magnitude of the hybridized transition dipole modulus of the dimer system is a function of the orientation of the rods in the dimer. This value can be calculated by summing the oscillator frequencies or the two rods. The oscillator frequency (f) is directly proportional to the square of the transition dipole modulus (μ), where the modulus is a function of the rotation angle of the one nanorod as it is rotated around its center of mass.

$$\mu = \varepsilon_m \hat{E} \alpha \tag{5}$$

In eq 5, ε_m is the electric permittivity of the medium, $\hat{E}$ is the incident electric field applied to the nanoparticle system, and α is the dipole polarizability of the nanoparticle, shown in eq 6

$$\alpha = 3\varepsilon_0\left(\frac{\varepsilon - \varepsilon_m}{\varepsilon + \kappa^*\varepsilon_m}\right)V \tag{6}$$

Here, ε is the dielectric permittivity of the nanoparticle material, κ is a shape dependent variable, and V is the volume of the particle.

The total oscillator frequency (f_T) of the nanorod dimer can be calculated by summing the component oscillator frequencies of each dimer pair:

$$f_{TOT} = f_1\cos\theta_1 + f_2\cos\theta_2 \tag{7}$$

For all dimers in this work, $f_1 = f_2$ since the nanorods in the dimer are identical. In the case where the nanorods are oriented tip-to-tip, $\theta_1 = \theta_2 = 0$ and $f_{TOT} = f_1 + f_2 = 2f$. In the case where one nanorod is rotated by some angle θ away from the interparticle axis, the os-

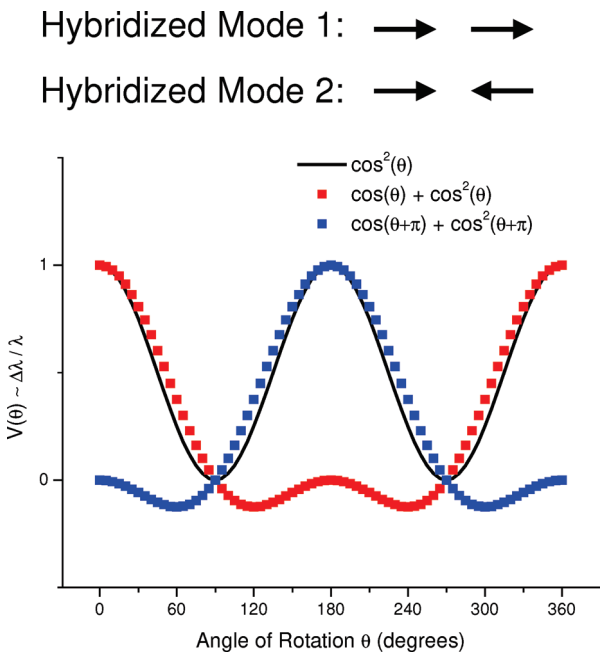

Figure 5. Close agreement between $\cos^2(\theta)$, which fits the data in Figure 4 (black line) and the mathematically derived full functional dependence of the plasmonic hybridized energy level (fractional shift in the plasmonic resonance wavelength) on rotation angle of one nanorod around a central pivot point. There are two hybridized modes, antisymmetric at $\theta = 0$ (HM1) and symmetric at $\theta = 0$ (HM2). The only resonance shift occurs when the dipoles are constructively interfering.

cillator strength along that axis is reduced by a factor $\cos\theta$, and $f_{TOT} = f(1 + \cos\theta) = 2f$. Therefore, the square of the allowed component of the total dipole transition modulus is expressed in eq 8.

$$\mu^2_{TOT} \propto f_{TOT} = f(1 + \cos\theta) \quad (8)$$

The full dependence of the hybridized energy separation on the rotation of one nanorod in a nanorod dimer away from the interparticle axis by θ is thus

$$V[\theta] = |1 + \cos\theta| \times |\cos\theta| = |\cos\theta + \cos^2\theta| \quad (9)$$

In summary, the two contributions ($|1 + \cos\theta|$ and $|\cos\theta|$) to the rotational dependence in eq 9 originate from (1) the induced transition dipole (μ) coupled with the incident field polarization and (2) the orientation factor κ, which accounts for the coupling between the two fields with respect to one another. As mentioned previously, MECT predicts that the degenerate excited states of excitons in a dimer are split into two energy levels, one at higher energy and one at lower corresponding to the symmetric and antisymmetric relative dipole orientations, respectively (shown in Figure 2). Equation 9 is plotted in Figure 5 for hybridized mode 1 (antisymmetric mode) and hybridized mode 2 (symmetric mode) and is shown to very nearly overlap with the $\cos^2\theta$ dependence fit to the data in Figure 4C (black line). Note that due to symmetry hybridized mode 2 is 180° out of phase with hybridized mode 1.

The diagram in Figure 2B depicts two plasmonic resonance modes at different energy levels. We have predominately discussed the antisymmetric mode (lower energy) of the dimer system so far in this article. The symmetric mode (higher energy) is often referred to as the "dark plasmon" mode since the net dipole moment of the system is zero[32] and is not spectroscopically observable. Upon rotation of one nanoparticle, the net dipole of the dark plasmon becomes non-zero. However, this resonance mode remains unobservable here in the experimental and simulation, which is consistent with the mathematical derivation in eq 9, as the constructively coupling mode (HM1 when $0 < \theta < 90°$ and $270 < \theta < 360°$; HM2 when $90 < \theta < 270°$) is the dominant mode. This is more clearly observed in Figure 5 where the contribution to the energy shift of the destructively coupling mode is very small.

Effect of the Dipolar Modulus on Plasmonic Coupling. An important issue of the plasmonic nanoparticle ruler application has been the report of a slower decay of the plasmonic coupling than predicted by either the exponential or R^{-3} relationships. This can be observed in the spectra reported here (Figure 1D) and many other reported simulation and experimental data sets,[17,21,24] generally around $R/D \sim 2$. Additionally, it was pointed out that at very small interparticle separations (surface-to-surface separations <5 nm) the lower energy hybridized plasmonic band shifts more rapidly to lower energy than is predicted by the single exponential function used by many groups.[19] Both of these phenomena need to be accounted for to obtain a more practical model of the plasmonic near-field coupling. The Simpson−Peterson approximation (eq 3) indicates that the shift in energy from the monomer excited dipole energy to the hybridized excited dipole energy is proportional to the square modulus of the transition dipole for MECT. However, for near-field plasmonic coupling, the *x*-component of the transition dipole (along the interparticle axis and parallel with the electric field of light) increases nearly exponentially as the separation between nanoparticles decreases (not shown), due to increased coupling between the dipole and quadrupole modes. Qualitatively, this phenomenon explains the increased energy shift in the hybridized excited plasmon resonance compared with the R^{-3} dependence for two coupling dipoles.

Recently, we published an article investigating the near-field dipole coupling between nanoprisms[17] and the induced energy shift of the hybridized excited plasmonic mode. We reported that the range of plasmonic coupling was larger for nanoprisms compared to nanospheres and nanodiscs of comparable size. This was quantitatively measured by the decay length of the plasmonic coupling (τ) using the best-fit exponential decay function and was quantitatively reported to be

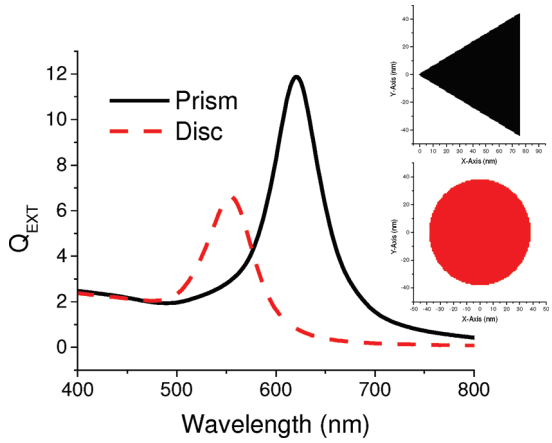

Figure 6. Comparison of the extinction intensity of a nanodisc (red dashed) and a nanoprism (black solid). The intensity of the dipole plasmonic mode is ~80% stronger for the nanoprism than for the nanodisc, and thus the nanoprism transition dipole modulus is roughly 80% greater. The sizes of the particles are comparable (bisector = diameter = 75 nm, height = 20 nm), and the dipole spacing in both cases is 1 nm.

50% larger in prisms ($\tau = 0.35$) compared to discs ($\tau = 0.22$). Pragmatically, this means that nanoprisms have a larger measurement range than nanodiscs and nanospheres with comparable sizes, and smaller particles can be used which lead to less perturbation in the substrate. This result is qualitatively explained by comparing the transition dipole modulus of the nanoprism to the transition dipole modulus of the nanodisc of relatively the same size. Using the DDA method, we have compared the transition dipole moduli of these two shapes in Figure 6, which is directly proportional to the intensity of the extinction band. The simulated nanoprism and nanodisc shapes both had a size of 75 nm, which corresponds to the respective bisector and diameter, and a thickness of 20 nm (inset of Figure 6). The intensity of the dipole resonance extinction band for the nanoprism is roughly 80% larger than that of the nanodisc of equal size. Thus, the fractional shift in the hybridized plasmonic mode for two nanoprisms will be more strongly shifted at a given interparticle separation than for two nanodiscs, for equally sized particles.

There has been a recent publication from our group[33] describing the affect of varying the dielectric medium of the nanoparticles on the sensitivity or degree of plasmonic field coupling. This report indicates that the near-field dipole coupling between particles increases with an increasing dielectric medium. This conclusion is consistent with the Simpson−Peterson approximation. The hybridized energy shift is predicted to be inversely proportional to the square of the refractive index of the medium and directly proportional to the transition dipole modulus. As defined in eq 5, the transition dipole modulus is directly proportional to the electric permittivity of the medium (ε_m), which is nearly equal to the square of the refractive index of the medium in the limit of the magnetic permeability equal to 1. Thus the full dependence of the hybridized energy shift (V) on the refractive index of the medium should be $U \propto \eta^2$.

With these considerations, in addition to the orientation and separation results discussed in the previous sections, the Simpson−Peterson approximation that quantitatively describes the hybridized energy level splitting in MECT can be modified to approximate the hybridized energy level splitting between near-field coupled plasmonic fields. Equation 10 gives the modified version of this equation for identical nanoparticles:

$$V \approx \frac{\Delta\lambda}{\lambda} \propto \eta^2 \times |\mu^2| \times |\kappa| \times \Gamma \qquad (10)$$

where η is the refractive index of the medium, μ is the transition dipole module, κ is the orientation factor and is defined as

$$\kappa = \varphi^*(\cos\theta_{12} - 3\cos\theta_{1R}\cos\theta_{2R}) \text{ and } \varphi = (\cos\theta_{1P} + \cos\theta_{2P}) \qquad (11)$$

where 1 and 2 represent the axis of the induced plasmonic dipole, R is the interparticle axis, and P is the polarization axis of the light. The last term in eq 10 represents the functional dependence on the separation of the plasmonic fields. Several different functions can be used, including an exponential eq 1 or a more complex but fundamentally derived fit, for example, eq 3.

The two functions presented here (eq 1 and 2) are limited in scope and have certain drawbacks that must be considered when using them. The exponential fit is only a near approximation and has a poor fit when $1.5 < R/D < 2.5$, while eq 3 has two variables that must be accurately computed for the shape of the particle. Both equations must be taken as approximations only above moderate separations ($s > 1.1*D$) since below this separation the coupling increases more rapidly than either model predicts, due to higher order multipole coupling. Future work should focus on analytically deriving this function that includes higher order multipole coupling and the influence of separation on the transition dipole module, μ. This would prove to be a beneficial addition to the model and assist toward the integration of plasmonic nanoparticles in applications.

CONCLUSION

In conclusion, we report that the near-field electromagnetic coupling of two plasmonic nanorods can be modeled as a function of orientation by using the κ function that is taken from the Simpson−Peterson approximation that is used in MECT. The plasmonic field coupling was experimentally shown to have approximately a $\cos^2\theta$ dependence on the orientation of one nanorod with respect to a neighboring nanorod, where θ is the angle between the interparticle axis and the axis of the longitudinal plasmonic mode of the rotated nanorod. This relationship was also theoretically confirmed using DDA simulations. A model equation was

presented, based on the Simpson−Peterson approximation, whereby the coupling of the plasmonic fields is a function of four variables, namely, the the separation between nanoparticles, the transition dipole module induced, the refractive index of the medium, and the relative orientations of the nanoparticles. In agreement with previous DDA work,[17] the best-fit exponential decay length was experimentally verified to be $\tau =$ 0.22 in units of the nanorod length. From this work, we present some of the first systematic studies of orientation dependence of the plasmonic coupling between two nanoparticles, identifying a new method to not only map nanometer distances in 1 dimension but also to potentially expand the application to a powerful two- or three-dimensional mapping technique solely utilizing optical spectra of the nanoparticles.

EXPERIMENTAL SECTION

Nanorod arrays were fabricated using a JEOL JBX-9300FS 100 kV electron beam lithography (EBL) system. The substrates used to support the nanoprisms were prefabricated free-standing silicon nitride membranes whose fabrication has been described in detail elsewhere.[34] Briefly, silicon wafers with a ⟨100⟩ orientation were purchased from University Wafer and cleaned and placed in a Tystar Furnace. Si_3N_4 was deposited onto the wafer surface using a low-pressure chemical vapor deposition process at a deposition rate of 5 nm/min to a final thickness of 50 ± 3 nm. A combination of optical photolithography and dry etching with CF_4 removed selected areas of the membrane from one side of the wafer. These areas were exposed to KOH to anisotropically etch the silicon wafer through to the other side, exposing the other silicon nitride membrane. This process produced an array of silicon nitride membrane windows freely supported that were 150 × 150 μm^2. Each window was used for a single design pattern, and each pattern array was 300 × 300 μm^2 in order to ensure pattern overlap with the window. A poly(methyl methacrylate) (PMMA) positive electron resist was spin coated onto the top Si_3N_4 side of the wafer to a thickness of 80 nm. A dose of 2750 $\mu C/cm^2$ was used to write the pattern at a beam current of 1.98 nA. Development of the exposed areas was carried out in a 1:3 methyl isobutyl ketone/isopropyl alcohol (MIBK/IPA) solution for 10 s. The sample was then washed in IPA for 30 s before gently drying in a stream of N_2. A thin chrome layer (0.5 nm @ 0.1 Å/s) was evaporated onto the sample using a CVC electron beam evaporator followed by a 20.0 nm layer of gold at a rate of 0.5 Å/s. The Cr served as an adhesion layer between the Si_3N_4 surface and the Au nanoparticles. Final lift-off and removal of the PMMA mask was accomplished by placing the sample in 1165 remover purchased from MicroChem for 24 h. The array was designed so that the nanoparticle dimer pairs were spaced more than 800 nm from one another to reduce far-field coupling that has been observed by Rechberger *et al.*[22] in 150 nm diameter gold nanodisc arrays. This far-field coupling has been shown by the Moerner group to exist at large separations (5−7 particle lengths). For this reason, individual particle dimers were experimentally spaced no less than 8 particle diameters apart, and no interparticle separations were used greater than 5 particle lengths. In these experimental samples with small interparticle gaps (20−300 nm), the near-field coupling can be expected to be much stronger than any far-field grating effects.

The supported nanorods were imaged using a Zeiss Ultra60 scanning electron microscope (SEM). Extinction measurements were performed on a Craic 1100 microspectrophotometer in transmission mode under polarized light (along the interparticle axis) using a 5× magnification. The collection spot was ~32.0 × 32.0 μm^2, and several different areas were collected from the center of the array and averaged to produce the reported spectra. A comparison between magnified SEM images from various membrane windows shows excellent homogeneity in the particle shapes and sizes as the spacing and orientation is varied.

The optical response of the nanoparticle dimer systems has been calculated using the DDA method with the DDSCAT 6.1 code publicly offered by Draine and Flatua[35] and modified by Goodman[36] and Schatz.[37] The method has been described in great detail elsewhere.[38] Briefly, the method approximates the desired particle shape as a three-dimensional cubic lattice of polarizable point dipoles of preprogrammed dipole−dipole spacing. The program solves for the scattering and absorption of each polarizable point self-consistently in response to an incident plane polarized field and polarization of neighboring dipole points. The bulk values of the dielectric constants reported by Johnson and Christy[39] for gold were used. The DDA method has been demonstrated by many groups[40−43] to be suitable for optical calculations of the extinction spectrum and the local electric field distribution in metal particles with different geometries and environments. The incident light is always polarized parallel with the interparticle axis in this report, and the dielectric of the host medium was set at $\varepsilon_m = 1.00$. As discussed by Rechberger *et al.*,[22] it is reasonable to consider the calculations of a single particle pair instead of the entire 2-D array. This consideration is justifiable because the particle pairs in the experiment are separated from each other by large distances on the order of eight particle diameters, large enough so that no coupling occurs between different particle pairs. This ensures that only the interactions between the two particles within the dimer are measured.

Acknowledgment. This work was supported by the Division of Materials Research of the National Science Foundation (No. 0138391). We thank B. T. Draine and P. J. Flatau for use of their DDA code, DDSCAT 6.1, and Professor C. Henderson's lab for supplying the Si_3N_4 substrates.

REFERENCES AND NOTES

1. Choi, M.-R.; Stanton-Maxey, K. J.; Stanley, J. K.; Levin, C. S.; Bardhan, R.; Akin, D.; Badve, S.; Sturgis, J.; Robinson, J. P.; Bashir, R.; *et al.* A Cellular Trojan Horse for Delivery of Therapeutic Nanoparticles into Tumors. *Nano Lett.* **2007**, *7*, 3759–3765.
2. Gobin, A. M.; Lee, M. H.; Halas, N. J.; James, W. D.; Drezek, R. A.; West, J. L. Near-Infrared Resonant Nanoshells for Combined Optical Imaging and Photothermal Cancer Therapy. *Nano Lett.* **2007**, *7*, 1929–1934.
3. Huang, X.; El-Sayed, I. H.; Qian, W.; El-Sayed, M. A. Cancer Cell Imaging and Photothermal Therapy in the Near-Infrared Region by Using Gold Nanorods. *J. Am. Chem. Soc.* **2006**, *128*, 2115–2120.
4. Huang, W.; Qian, W.; El-Sayed, M. A. Gigahertz Optical Modulation Resulting from Coherent Lattice Oscillations Induced by Femtosecond Laser Pumping of 2d Photonic Crystals of Gold-Capped Polystyrene Microspheres. *Adv. Mater.* **2008**, *20*, 733–737.
5. Lin, A.; Boo, S.; Moon, D. S.; Jeong, H. J.; Chung, Y.; Han, W.-T. Luminescence Enhancement by Au Nanoparticles in Er^{3+}-Doped Germano-Silicate Optical Fiber. *Opt. Express* **2007**, *15*, 8603–8608.
6. Maier, S. A.; Brongersma, M. L.; Kik, P. G.; Meltzer, S.; Requicha, A. A. G.; Atwater, H. A. Plasmonics—A Route to Nanoscale Optical Devices. *Adv. Mater.* **2001**, *13*, 1501–1505.
7. Maier, S. A.; Kik, P. G.; Atwater, H. A.; Meltzer, S.; Harel, E.; Koel, B. E.; Requicha, A. A. G. Local Detection of Electromagnetic Energy Transport below the Diffraction Limit in Metal Nanoparticle Plasmon Waveguides. *Nat. Mater.* **2003**, *2*, 229–232.

8. Jiang, J.; Bosnick, K.; Maillard, M.; Brus, L. Single Molecule Raman Spectroscopy at the Junctions of Large Ag Nanocrystals. *J. Phys. Chem. B* **2003**, *107*, 9964–9972.
9. Nikoobakht, B.; El-Sayed, M. A. Surface-Enhanced Raman Scattering Studies on Aggregated Gold Nanorods. *J. Phys. Chem. A* **2003**, *107*, 3372–3378.
10. Rosi, N. L.; Mirkin, C. A. Nanostructures in Biodiagnostics. *Chem. Rev.* **2005**, *105*, 1547–1562.
11. Willets, K. A.; Van Duyne, R. P. Localized Surface Plasmon Resonance Spectroscopy and Sensing. *Annu. Rev. Phys. Chem.* **2007**, *58*, 267–297.
12. Zou, S.; Schatz, G. C. Silver Nanoparticle Array Structures That Produce Giant Enhancements in Electromagnetic Fields. *Chem. Phys. Lett.* **2005**, *403*, 62–67.
13. Jain, P. K.; Eustis, S.; El-Sayed, M. A. Plasmon Coupling in Nanorod Assemblies: Optical Absorption, Discrete Dipole Approximation Simulation, and Exciton-Coupling Model. *J. Phys. Chem. B* **2006**, *110*, 18243–18253.
14. Prodan, E.; Radloff, C.; Halas, N. J.; Nordlander, P. A. Hybridization Model for the Plasmon Response of Complex Nanostructures. *Science* **2003**, *302*, 419–422.
15. Packard, B. Z.; Toptygin, D. D.; Komoriya, A.; Brand, L. Intramolecular Resonance Dipole−Dipole Interactions in a Profluorescent Protease Substrate. *J. Phys. Chem. B* **1998**, *102*, 752–758.
16. Kasha, M.; Rawls, H. R.; El-Bayoumi, M. A. Exciton Model in Molecular Spectroscopy. *Pure Appl. Chem.* **1965**, *11*, 371–92.
17. Tabor, C.; Murali, R.; Mahmoud, M.; El-Sayed, M. A. On the Use of Plasmonic Nanoparticle Pairs as a Plasmon Ruler: The Dependence of the Near-Field Dipole Plasmon Coupling on Nanoparticle Size and Shape. *J. Phys. Chem. A* **2009**, *113*, 1946–1953.
18. Haynes, C. L.; Van Duyne, R. P. Nanosphere Lithography: A Versatile Nanofabrication Tool for Studies of Size-Dependent Nanoparticle Optics. *J. Phys. Chem. B* **2001**, *105*, 5599–5611.
19. Funston, A. M.; Novo, C.; Davis, T. J.; Mulvaney, P. Plasmon Coupling of Gold Nanorods at Short Distances and in Different Geometries *Nano Lett.* **2009**, *9*, 1651−1658.
20. Su, K. H.; Wei, Q. H.; Zhang, X.; Mock, J. J.; Smith, D. R.; Schultz, S. Interparticle Coupling Effects on Plasmon Resonances of Nanogold Particles. *Nano Lett.* **2003**, *3*, 1087–1090.
21. Jain, P. K.; Huang, W.; El-Sayed, M. A. On the Universal Scaling Behavior of the Distance Decay of Plasmon Coupling in Metal Nanoparticle Pairs: A Plasmon Ruler Equation. *Nano Lett.* **2007**, *7*, 2080–2088.
22. Rechberger, W.; Hohenau, A.; Leitner, A.; Krenn, J. R.; Lamprecht, B.; Aussenegg, F. R. Optical Properties of Two Interacting Gold Nanoparticles. *Opt. Commun.* **2003**, *220*, 137–141.
23. Jain, P. K.; El-Sayed, M. A. Universal Scaling of Plasmon Coupling in Metal Nanostructures: Extension from Particle Pairs to Nanoshells. *Nano Lett.* **2007**, *7*, 2854–2858.
24. Jain, P. K.; El-Sayed, M. A. Surface Plasmon Coupling and Its Universal Size Scaling in Metal Nanostructures of Complex Geometry: Elongated Particle Pairs and Nanosphere Trimers. *J. Phys. Chem. C* **2008**, *112*, 4954–4960.
25. Willingham, B.; Brandl, D. W.; Nordlander, P. Plasmon Hybridization in Nanorod Dimers. *Appl. Phys. B* **2008**, *93*, 209–216.
26. Reinhard, B. M.; Siu, M.; Agarwal, H.; Alivisatos, A. P.; Liphardt, J. Calibration of Dynamic Molecular Rulers Based on Plasmon Coupling between Gold Nanoparticles. *Nano Lett.* **2005**, *5*, 2246–2252.
27. Dionne, J. A.; Verhagen, E.; Polman, A.; Atwater, H. A. Are Negative Index Materials Achievable with Surface Plasmon Waveguides? A Case Study of Three Plasmonic Geometries. *Opt. Express* **2008**, *16*, 19001–19017.
28. Oulton, R. F.; Sorger, V. J.; Genov, D. A.; Pile, D. F. P.; Zhang, X. A Hybrid Plasmonic Waveguide for Subwavelength Confinement and Long-Range Propagation. *Nat. Photonics* **2008**, *2*, 496–500.
29. Rusina, A.; Durach, M.; Nelson, K. A.; Stockman, M. I. Nanoconcentration of Terahertz Radiation in Plasmonic Waveguides. *Opt. Express* **2008**, *16*, 18576–18589.
30. Joseph, S. T. S.; Ipe, B. I.; Pramod, P.; Thomas, K. G. Gold Nanorods to Nanochains: Mechanistic Investigations on Their Longitudinal Assembly Using α.ω-Alkanedithiols and Interplasmon Coupling. *J. Phys. Chem. B* **2006**, *110*, 150–157.
31. Thomas, K. G.; Barazzouk, S.; Ipe, B. I.; Joseph, S. T. S.; Kamat, P. V. Uniaxial Plasmon Coupling through Longitudinal Self-Assembly of Gold Nanorods. *J. Phys. Chem. B* **2004**, *108*, 13066–13068.
32. Hao, F.; Larsson, E. M.; Ali, T. A.; Sutherland, D. S.; Nordlander, P. Shedding Light on Dark Plasmons in Gold Nanorings. *Chem. Phys. Lett.* **2008**, *458*, 262–266.
33. Jain, P. K.; El-Sayed, M. A. Noble Metal Nanoparticle Pairs: Effect of Medium for Enhanced Nanosensing. *Nano Lett.* **2008**, *8*, 4347–4352.
34. Lee, C.-T.; Wang, M.; Jarnagin, N. D.; Gonsalves, K. E.; Roberts, J. M.; Wang, Y.; Henderson, C. L. Photosensitivity and Line-Edge Roughness of Novel Polymer-Bound Pag Photoresists. *Proc. SPIE-Int. Soc. Opt. Eng.* **2007**, *6519*, 65191E/1–65191E/9.
35. Flatau, P. J.; Stephens, G. L.; Draine, B. T. Light Scattering by Rectangular Solids in the Discrete-Dipole Approximation: A New Algorithm Exploiting the Block-Toeplitz Structure. *J. Opt. Soc. Am.* **1990**, *7*, 593–600.
36. Goodman, J. J.; Draine, B. T.; Flatau, P. J. Application of Fast-Fourier-Transform Techniques to the Discrete-Dipole Approximation. *Opt. Lett.* **1991**, *16*, 1198–200.
37. Shuford, K. L.; Ratner, M. A.; Schatz, G. C. Multipolar Excitation in Triangular Nanoprisms. *J. Chem. Phys.* **2005**, *123*, 114713/1–114713/9.
38. Kelly, K. L.; Coronado, E.; Zhao, L. L.; Schatz, G. C. The Optical Properties of Metal Nanoparticles: The Influence of Size, Shape, and Dielectric Environment. *J. Phys. Chem. B* **2003**, *107*, 668–677.
39. Johnson, P. B.; Christy, R. W. Optical Constants of the Noble Metals. *Phys. Rev. B* **1972**, *6*, 4370–4379.
40. Brioude, A.; Jiang, X. C.; Pileni, M. P. Optical Properties of Gold Nanorods: DDA Simulations Supported by Experiments. *J. Phys. Chem. B* **2005**, *109*, 13138–13142.
41. Lee, K.-S.; El-Sayed, M. A. Dependence of the Enhanced Optical Scattering Efficiency Relative to That of Absorption for Gold Metal Nanorods on Aspect Ratio, Size, End-Cap Shape, and Medium Refractive Index. *J. Phys. Chem. B* **2005**, *109*, 20331–20338.
42. Schatz, G. C. Electrodynamics of Nonspherical Noble Metal Nanoparticles and Nanoparticle Aggregates. *THEOCHEM* **2001**, *573*, 73–80.
43. Wiley, B. J.; Im, S. H.; Li, Z.-Y.; McLellan, J.; Siekkinen, A.; Xia, Y. Maneuvering the Surface Plasmon Resonance of Silver Nanostructures through Shape-Controlled Synthesis. *J. Phys. Chem. B* **2006**, *110*, 15666–15675.